Am J Transl Res 2020;12(2):633-648
www.ajtr.org /ISSN:1943-8141/AJTR0100952

Original Article

Integrated bioinformatics analysis identifies microRNA-376a-3p as a new microRNA biomarker in patient with coronary artery disease

Lei Du[1*], Zhimin Xu[2*], Xuhui Wang[3], Fang Liu[1]

Departments of [1]Gerontology, [2]Cardiovascular Medicine, [3]Neurosurgery, Xinhua Hospital Affiliated to Shanghai Jiao Tong University School of Medicine, Shanghai 200092, P. R. China. [*]Equal contributors and co-first authors.

Received August 14, 2019; Accepted January 17, 2020; Epub February 15, 2020; Published February 28, 2020

Abstract: Introduction: Coronary artery disease (CAD) is a major global health problem with high incidence and mortality. Despite many advances in treatment, the prognosis of patients with CAD still remains poor. Therefore, this study aimed to identify potential biomarkers and targets associated with the progression of CAD. Methods: Two gene expression profile datasets (GSE20681 and GSE12288), and two microRNA (miRNA) expression profile datasets (GSE59421 and GSE105449) were downloaded from the Gene Expression Omnibus (GEO) database; R language was used to screen out the differentially expressed genes (DEGs) and differentially expressed miRNAs (DEMs), respectively. In addition, five online bioinformatics tools (miRWalk et al.) were used to identify the target genes of DEMs, and miRNA-gene network was constructed using Cytoscape software. Moreover, CCK-8, flow cytometry assays were used to detect the cell proliferation and apoptosis in human umbilical vein endothelial cells (HUVECs). Meanwhile, the dual luciferase reporter system assay was used to explore the interaction of miR-376a-3p and NRIP1 in HUVECs. Results: In the present study, 150 common DEGs and 5 common DEMs were screened using a Venn diagram in R language. First, a total of 6812 target genes were identified from the overlapping DEMs. Second, 26 overlapping dysregulated genes from 150 overlapping DEGs and 6812 miRNA target genes were identified. Meanwhile, 43 miRNA-gene regulatory pairs were obtained between the 5 common DEMs and 26 dysregulated genes. Downregulation of miR-376a-3p significantly inhibited the proliferation of HUVECs via inducing apoptosis. Moreover, overexpression of miR-376a-3p markedly inhibited the growth of HUVECs via downregulating NRIP1. Conclusion: In this study, miR-376a-3p-NRIP1 pair might involve in the progression of CAD, implying that miR-376a-3p may be a therapeutic target for the treatment of CAD.

Keywords: Coronary artery disease, gene expression omnibus, miR-376a-3p, NRIP1

Introduction

Cardiovascular disease (CVD) is the leading cause of death globally [1]. Coronary artery disease (CAD), also known as ischemic heart disease (IHD), is considered to be one of the most dangerous CVD. The mortality of CAD has been increasing enormously [1, 2]. Sudden cardiac death, stable angina, myocardial infarction, and unstable angina are the common types of CAD [3]. In addition, CAD is caused by the reduction of blood flow to the heart muscle due to accumulation of lipids and plaque in the arteries of the heart [4]. The common pathogenic factors of CAD are age, hypertension, obesity, high cholesterol, family history, smoking and sedentary lifestyle [5-7]. So far, the treatment options for patients with complex CAD included percutaneous coronary intervention or coronary artery bypass surgery [8]. However, the rate of mortality and rehospitalization are still high in patients with CAD [9]. Therefore, it is necessary to explore novel effective therapies for the early diagnosis and treatment of CAD.

In recent years, microarray has been effective in detecting the complex network during the process of atherosclerosis, and even in screening biomarkers for CAD diagnosis and prognosis [10]. It has been indicated that combination microarray technology with bioinformatics anal-

ysis method could comprehensively analyze the expression changes of genes from early to advanced stage in the development of coronary atherosclerosis [10]. Gene Expression Omnibus (GEO, http://www.ncbi.nlm.nih.gov/geo/) is a public database containing a large number of gene profiles in various diseases [11, 12]. In addition, the GEO dataset could be used to screen out differentially expressed genes (DEGs) and to establish gene regulatory networks [13]. Recently, Wang et al. analyzed the raw data (GSE128829 and GSE59421) from the GEO database, and identified potential therapeutic targets associated with CAD [14].

In this study, raw data from microarray analyses conducted on CAD samples and healthy controls were downloaded from the GEO database, including mRNA and miRNA expression profile datasets. Meanwhile, by using the bioinformatics analysis method, we might provide effective biomarker candidates for clinical trials and clinical practice.

Materials and methods

Data acquisition

Four datasets (GSE20681, GSE12288, GSE59421 and GSE105449) which contain the gene expression profile of CAD and healthy controls, were downloaded from GEO database (https://www.ncbi.nlm.nih.gov/geo/). The mRNA microarray data of 420 CAD patients and healthy controls (198 samples from GSE20681, 222 samples from GSE12288) were downloaded from GEO database. The microRNA (miRNA) microarray data of 150 CAD patients and healthy controls (70 samples from GSE59421, 80 samples from GSE105449) were downloaded from GEO database.

Microarray data mining

In this study, two microarray datasets (GSE20681, GSE12288) were used to identify differentially expressed genes (DEGs). In addition, the data from another two microarray datasets (GSE59421 and GSE105449) were used to identify differentially expressed miRNAs (DEMs). The DEGs and DEMs were screened using R language, respectively. An adjusted *P*-value <0.05 was set as criteria.

The mRNAs related to CAD were obtained by overlapping DEGs from two datasets (GSE20681, GSE12288). The miRNAs related to CAD were obtained by overlapping DEMs from two datasets (GSE59421 and GSE105449).

GO and KEGG enrichment analysis

Gene ontology (GO, http://www.geneontology.org/) and Kyoto Encyclopedia of Genes and Genomes (KEGG, http://www.genome.jp/kegg/) enrichment analysis were used to conduct the functional analysis and significant pathways of the DEGs. GO enrichment analysis was used to allocate protein biomarkers into their corresponding pathways at three levels: biological process, cellular component and molecular function.

Canonical pathway, diseases and bio functions enrichment analysis

The ingenuity pathway analysis (IPA) software program was used to assign genes according to their biological functions, canonical pathways. The, the indirect or direct interactions between genes were analyzed [15]. Based on the ingenuity® knowledge database of IPA, the DEGs and the potential pathways may involve in were analyzed by the Fisher exact test. These DEGs underwent canonical pathway enrichment, diseases and bio functions analysis in IPA. In canonical pathway enrichment analysis, the Z-score (standard score) value of each pathway was calculated by the multiple of up-regulation and down-regulation of DEGs. In diseases and bio functions enrichment analysis, the Z-score (standard score) value was calculated by the extent of activation and suppression of disease.

MiRNA-gene-network construction

Target genes of the DEMs were identified using online bioinformatics tools including miRWalk, miRanda, miRDB, RNA22, and TargetScan. To construct the interaction network between differential miRNAs and differential mRNAs, bioinformatics software Cytoscape 3.3.0 was used.

Cell culture and transfection

The Human umbilical vein endothelial cells (HUVECs) were purchased from American Type Culture Collection (ATCC, Rockville, MD, USA). Cells were incubated in Dulbecco's modified Eagle's medium (DMEM, Thermo Fisher Scientific, Waltham, MA, USA) containing 10% fetal

bovine serum (Thermo Fisher Scientific) and 100 units/ml penicillin/streptomycin at 37°C in a 5% CO_2 atmosphere.

MiR-376a-3p mimics, miR-376a-3p inhibitor were purchased from GenePharma (Shanghai, China). The miR-376a-3p mimics and miR-376a-3p inhibitor were transfected into HUVECs respectively using Lipofectamine 2000 (Thermo Fisher Scientific) according to the manufacturer's instructions. The culture medium containing 10% FBS was changed at 6 h after transfection, and the cells were then incubated for 72 h at 37°C.

RT-qPCR

Total RNA was isolated from HUVECs using the Trizol reagent (Thermo Fisher Scientific) according to the manufacturer's protocol. cDNA was synthesized using a PrimeScript RT reagent Kit (Promega, Madison, WI, USA). The qPCR was performed on an Applied Biosystems 7500 Real Time PCR System (Applied Biosystems, Foster City, CA, USA) with the SYBR Green PCR Mix kit (Thermo Fisher Scientific) according to the manufacturer's instructions. The PCR primers sequences were as follows: has-miR-376a-3p, forward: 5'-GGCATAGAGGAAAATCCACG-3'; reverse: 5'-CTCAACTGGTGTCGTGGAGTC-3'. U6, forward: 5'-CTCGCTTCGGCAGCACAT-3'; reverse: 5'-AACGCTTCACGAATTTGCGT-3'. The relative miRNA level was normalized to the internal control U6 using the $2^{-\Delta\Delta CT}$ method.

CCK-8 assay

Cell counting kit-8 (CCK-8, Dojindo, Tokyo, Japan) was applied to measure the viability of HUVECs. HUVECs (5×10^3 cells per well) were seed onto 96-well plate and incubated at 37°C overnight. After transfection with miR-376a-3p mimics or miR-376a-3p inhibitor, the cells were cultured for 24, 48 and 72 h, respectively. Later on, the cells were incubated with 10 μL CCK-8 reagent for another 2 h at 37°C. Then, the absorbance was measured using a microplate reader (Thermo Fisher Scientific) at 450 nm.

Immunofluorescence staining assay

After transfection with miR-376a-3p mimics or miR-376a-3p inhibitor, HUVECs were cultured for 72 h. Cells were fixed with 4% paraformaldehyde for 20 min at room temperature and then incubated with anti-human antibody against Ki67 (1:100, Abcam, Cambridge, MA, USA) overnight at 4°C. Then, the cells were incubated with secondary antibodies conjugated with fluorescent Alexa Fluor 488 (1:1000, Abcam) for 1 h 37°C. The nuclei were stained with DAPI (Thermo Fisher Scientific) for 5 min. The immunofluorescence was visualized under a laser confocal microscope (Olympus CX23 Tokyo, Japan).

Flow cytometry

Apoptosis in HUVECs were detected using an Annexin V-FITC apoptosis detection kit (Thermo Fisher Scientific). HUVECs were washed cold PBS and resuspended in binding buffer (BD Biosciences, Franklin Lake, NJ, USA). After that, the cells were stained with 5 μL propidium iodide (PI) and 10 μL Annexin V-FITC for 15 min at room temperature in the dark. Then, the number of apoptotic cells was analyzed by flow cytometer (BD FACSCanto II, BD Bioscience) and calculated using BD FACSCalibur system (FACScan; BD Biosciences).

Western blot assay

Total protein from HUVECs was extracted using RIPA buffer (Thermo Fisher Scientific) on ice. After that, protein concentration was detected by using BCA Protein Assay kit (Generay, Shanghai, China). Equal amounts of protein (40 μg per lane) were separated by 10% sodium dodecyl sulfate polyacrylamide gel (SDS-PAGE) electrophoresis, and then transferred onto a polyvinylidene fluoride membrane (PVDF, Millipore, Billerica, MA, USA). Later on, the membranes were blocked with 5% nonfat milk at room temperature for 1 h and then incubated with the primary antibodies against Bax (1:1000, Abcam), cleaved caspase 3 (1:1000, Abcam), NRIP1 (1:1000, Abcam), p-p65 (1:1000, Abcam), p-IκB (1:1000, Abcam) and β-actin (1:1000, Abcam) overnight at 4°C. The membranes were then incubated with horseradish peroxidase-conjugated goat anti-rabbit IgG secondary antibody (1:5000, Abcam) for 1 h at room temperature. Enhanced chemiluminescence detection system (Thermo Fisher Scientific) was used to develop signal. β-actin was used as an endogenous control.

Luciferase reporter assays

Wild-type (WT)-NRIP1 3'-UTR or mutated-type (MT)-NRIP1 3'-UTR plasmid was co-transfected

with miR-376a-3p mimics respectively using Lipofectamine 2000 (Invitrogen, Carlsbad, CA, USA). After 48 h of incubation, the luciferase activities were detected using a Dual-Luciferase Reporter Assay System (Promega Madison, WI, USA) with renilla luciferase activity as endogenous control.

Statistical analysis

Data are presented as mean ± standard deviation from triplicate experiments. Graphs were generated using GraphPad Prism software (version 7.0, La Jolla, CA, USA). Protein expression of Bax, cleaved caspase 3, Bcl-2, NRIP1, p-p65 and p-IκB, and the results of the CCK-8 assay and the apoptosis assay were analyzed by one-way analysis of variance (ANOVA) followed by Dunnett's test. *P*-value <0.05 was considered as a statistically significant.

Results

Identification of DEGs in GEO dataset

Raw data from two independent datasets (GSE12288 and GSE20681) were downloaded from GEO; DEGs were identified using R language. In total, 1471 DEGs (759 downregulated and 712 upregulated mRNAs), 5584 DEGs (2729 downregulated and 1855 upregulated mRNAs) were screened from the GSE12288 and GSE20681 datasets, respectively. The distinguishable mRNAs expression between CAD samples and healthy controls were displayed by heatmap visualization in **Figure 1A** and **1B**. Meanwhile, these DEGs were visualized in volcano plots (**Figure 1C** and **1D**). In addition, the intersect function indicated that 150 DEGs were commonly dysregulated (79 down- and 71 upregulated DEGs from two independent datasets) using a Venn diagram in R language (**Figure 1E**).

GO enrichment and KEGG pathway analyses

The DEGs analysis were conducted using GO and KEGG. The GO enrichment analyses indicated that DEGs were significantly related to molecular function of "miRNA binding" and "transcription factor binding" (**Figure 2A**). In addition, KEGG analysis results showed that DEGs were mainly enriched in "Alcoholism" and "Viral carcinogenesis" (**Figure 2B**).

Canonical pathway enrichment analysis and diseases and Bio functions enrichment analysis

IPA enriched 330 canonical pathways (P<0.05) in CAD, and the top 20 canonical pathways were showed in **Figure 3A**; the details of pathways were presented in **Table 1**. The most significant canonical pathways included "RAR activation", "AMPK signaling", "FLT3 signaling in hematopoietic progenitor cells", and "LPS-stimulated MAPK Signaling" (**Figure 3A**). In addition, the diseases and bio functions enrichment analysis were conducted using IPA. The top 20 diseases and bio functions that overlapping DEGs were displayed in **Figure 3B**. The details of functions analysis were presented in **Table 2** and we found the overlapping DEGs were mainly associated with "cellular development, cellular growth and proliferation", "organismal injury and abnormalities, reproductive system disease", and "cellular development, cellular growth and proliferation" (**Figure 3B**). The above results indicated that these DEGs may regulate the progression of CAD via multiple signaling pathways.

Identification of DEMs in GEO

Two datasets GSE59421 and GSE105449 were downloaded from GEO. Following pre-processing of the raw data, DEMs were identified using R language. In total, 69 DEMs (30 downregulated and 39 upregulated miRNAs), 26 DEMs (21 downregulated and 5 upregulated miRNAs) were screened from the GSE59421 and GSE105449, respectively. The distinguishable miRNAs expression between CAD samples and healthy controls were displayed by heatmap visualization in **Figure 4A** and **4B**. Meanwhile, the distribution of DEMs were presented by volcano plot (**Figure 4C** and **4D**). In addition, 5 DEMs were commonly dysregulated using a Venn diagram in R language (**Figure 4E**).

MiRNA-gene-network and module selection

Online bioinformatics tools miRWalk, miRanda, miRDB, RNA22, and TargetScan were used to predict target genes of overlapping DEMs (**Figure 5A**). Meanwhile, overlapping dysregulated genes from overlapping DEGs and miRNA target genes were identified (**Figure 5A**). Furthermore, the interaction network of the overlapping dysregulated genes and 5 common

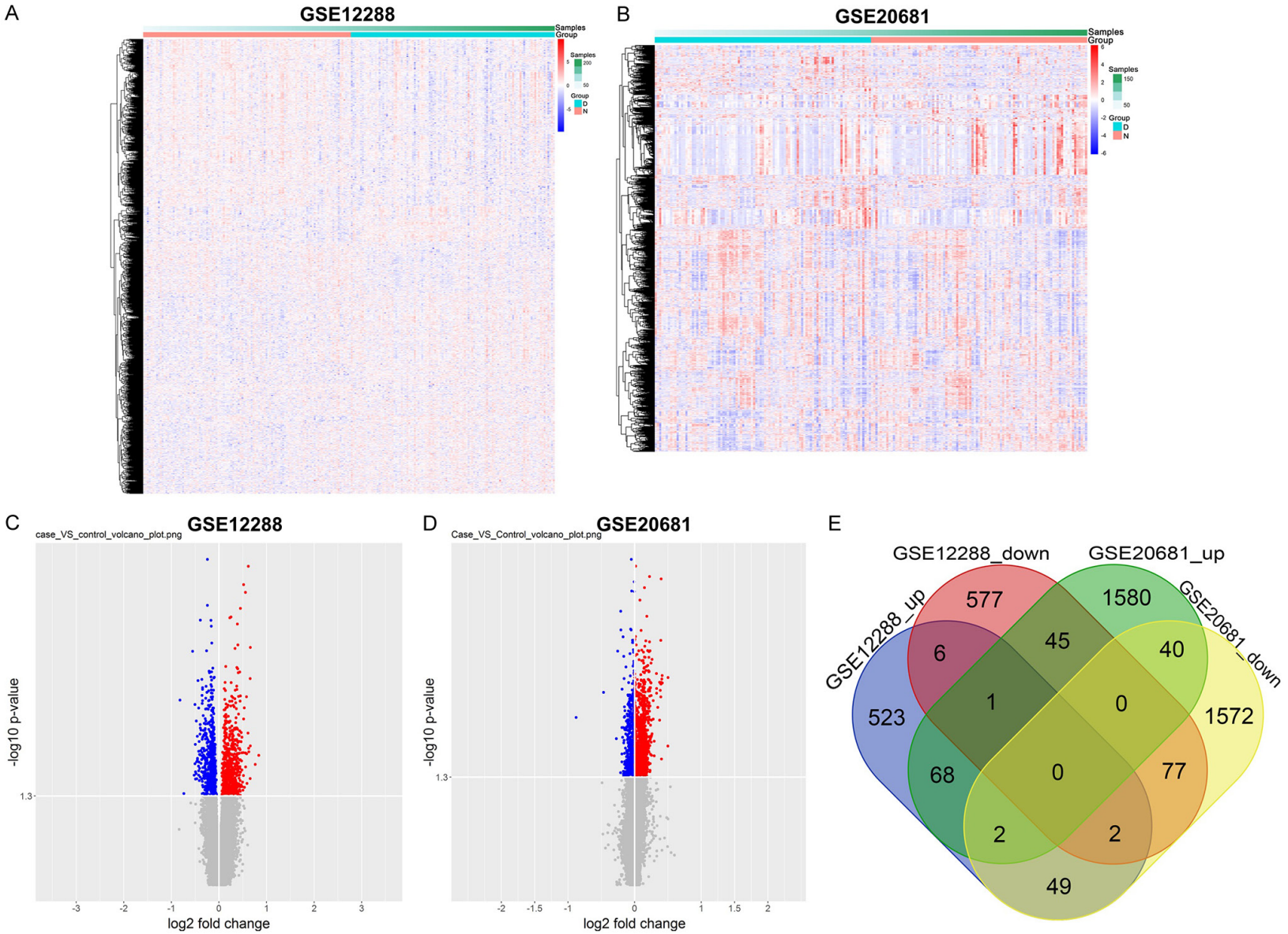
A
GSE12288
Samples
Group
B
GSE20681
Samples
Group
C
GSE12288
case_VS_control_volcano_plot.png
-log10 p-value
log2 fold change
D
GSE20681
Case_VS_Control_volcano_plot.png
-log10 p-value
log2 fold change
E
GSE12288_down
GSE20681_up
GSE12288_up
GSE20681_down
577
1580
523
1572
6
45
40
1
0
68
0
77
2
2
49

Figure 1. Identification of DEGs in GEO. Heat map showed the mRNA expression profiles of CAD samples and healthy controls according to *P* value, which downloaded from (A) GSE12288 dataset and (B) GSE20681 dataset. Red represents up-regulation, and blue indicates down-regulation. (C) Volcano plot of DEGs in GSE12288. (D) Volcano plot of DEGs in GSE20681. Gray, red and blue color represented relatively equal, high and low expression of genes respectively based on the cut-off values of |log2 fold change| >0 and -log10 (*p*-value) >1.3. (E) Venn diagram of overlapping DEGs from intersection of two independent datasets GSE12288 and GSE20681. A total of 91 upregulated and 79 downregulated overlapping DEGs was identified. Different colored regions represent different datasets.

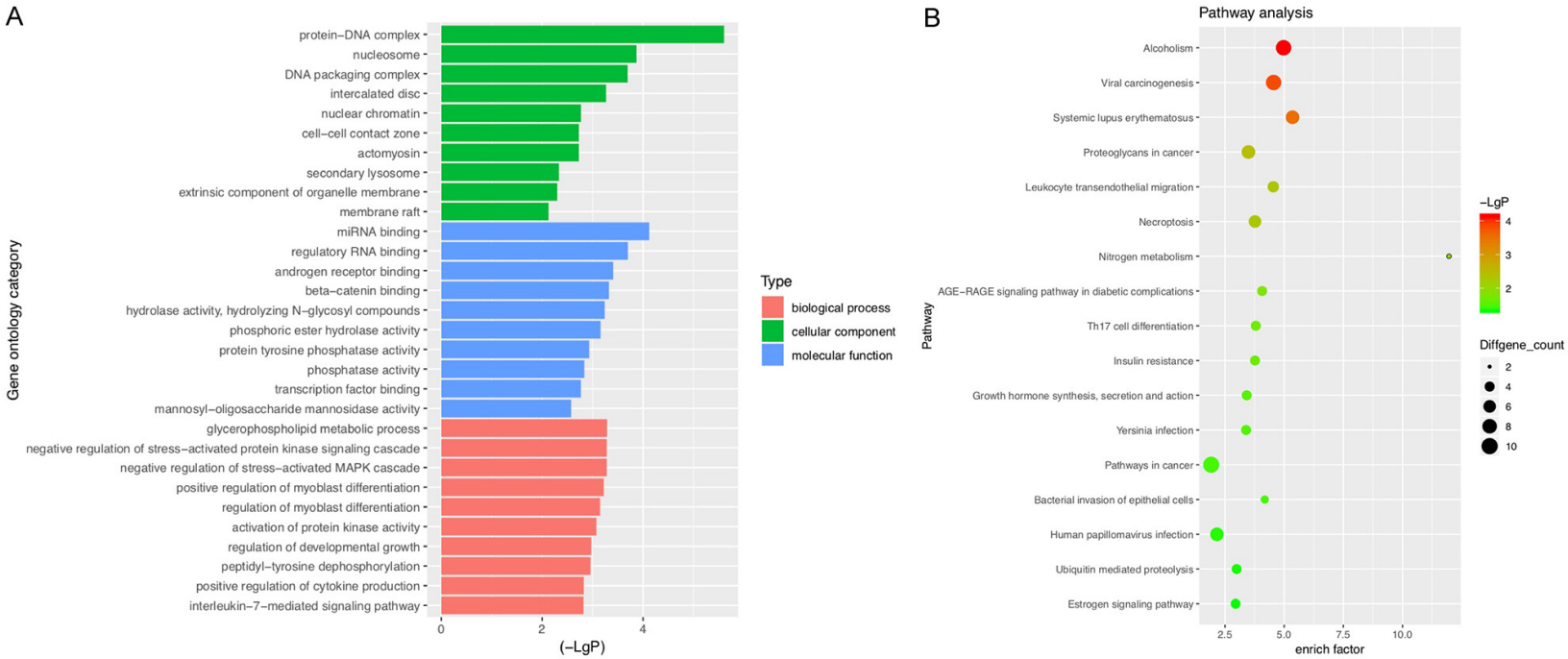

Figure 2. GO enrichment and KEGG pathway analyses. A. Overlapping DEGs were measured by GO enrichment analysis. B. Overlapping DEGs were measured by KEGG pathway analysis.

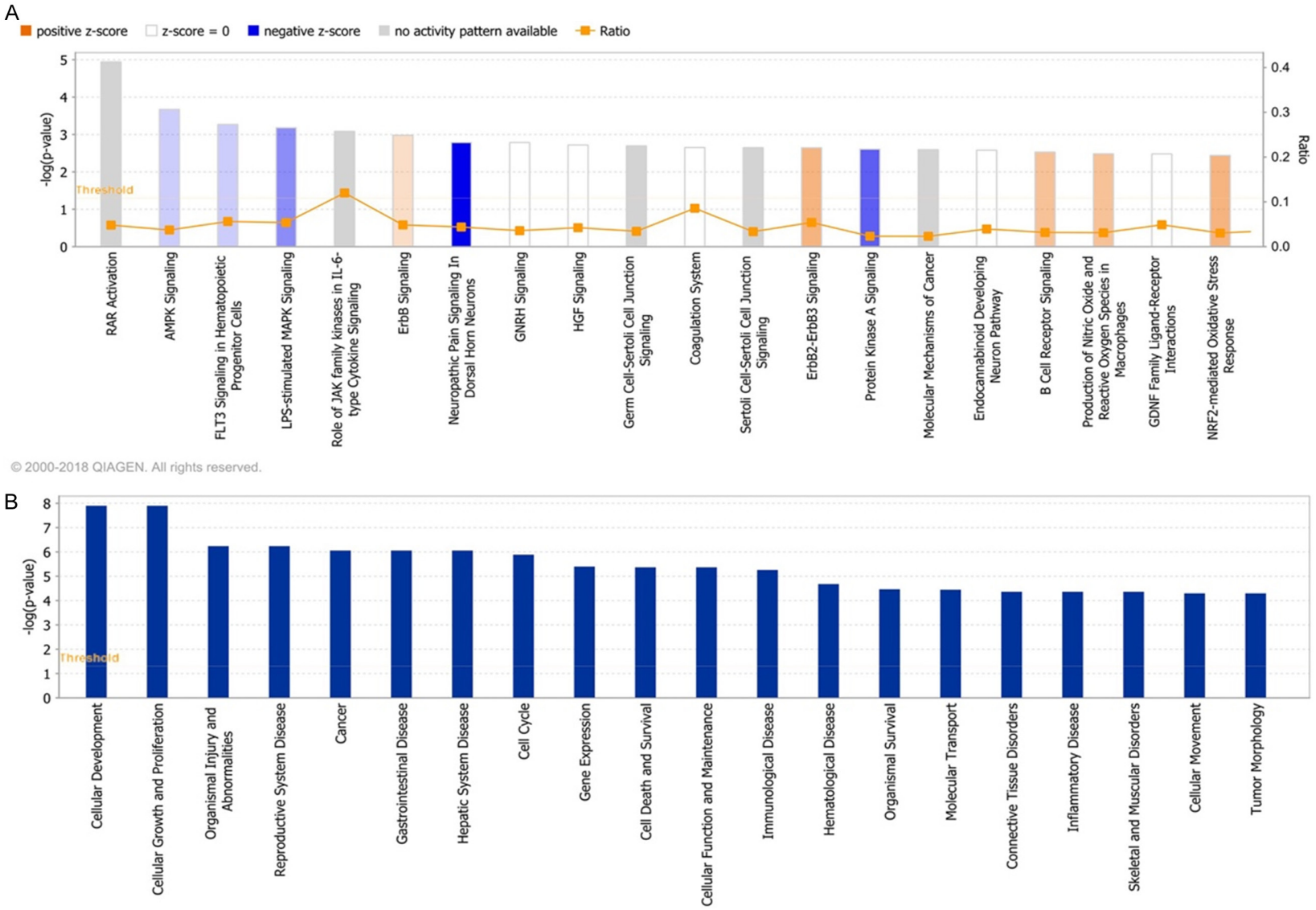

Figure 3. Canonical pathway enrichment analysis and Diseases and Bio functions enrichment analysis. A. Top 20 canonical pathways enriched in CAD. IPA software ranked the top canonical pathways based on -log (*p*-value). The yellow line represented P = 0.05. The columns that over the orange line denoted significant pathway in CAD. The orange broken line represented the Ratio value, which means the enrichment of the pathway. Orange and blue color in column represented pathway activation and pathway inhibition. B. Top 20 diseases and bio functions enriched in CAD. IPA software ranked the top diseases and bio functions based on -log (*p*-value). The yellow line represented P = 0.05. The columns that over the orange line denoted significant diseases and bio functions in CAD.

Table 1. Enrichment analysis table of canonical pathway

Ingenuity Canonical Pathways	log (*p*-value)	Ratio	z-score
RAR Activation	4.94	0.0481	#NUM!
AMPK Signaling	3.67	0.0372	-0.447
FLT3 Signaling in Hematopoietic Progenitor Cells	3.27	0.0562	-0.447
LPS-stimulated MAPK Signaling	3.18	0.0538	-1
Role of JAK family kinases in IL-6-type Cytokine Signaling	3.08	0.12	#NUM!
ErbB Signaling	2.98	0.0485	0.447
Neuropathic Pain Signaling In Dorsal Horn Neurons	2.79	0.0439	-2.236
GNRH Signaling	2.79	0.0357	0
HGF Signaling	2.72	0.0424	0
Germ Cell-Sertoli Cell Junction Signaling	2.69	0.0343	#NUM!
Coagulation System	2.65	0.0857	#NUM!
Sertoli Cell-Sertoli Cell Junction Signaling	2.65	0.0335	#NUM!
ErbB2-ErbB3 Signaling	2.64	0.0541	1
Protein Kinase A Signaling	2.61	0.0233	-1.414
Molecular Mechanisms of Cancer	2.59	0.0232	#NUM!
Endocannabinoid Developing Neuron Pathway	2.58	0.0394	0
B Cell Receptor Signaling	2.53	0.0317	0.816
Production of Nitric Oxide and Reactive Oxygen Species in Macrophages	2.48	0.0311	0.816
GDNF Family Ligand-Receptor Interactions	2.48	0.0488	0
NRF2-mediated Oxidative Stress Response	2.44	0.0305	1

DEMs were constructed using cytoscape 3.3.0 (**Figure 5B**). The results suggested that 6 genes including FN1, CREB1, NRIP1, PAFAH1B1, STAT5A and FKBP1A were identified as hub genes (**Table 3**). Meanwhile, as shown in **Figure 5B**, the 43 regulatory pairs between DEMs and their target genes were identified including has-miR-376a-3p-NRIP1. ROC analysis was performed to evaluate the miR-376a-3p expression between patients with CAD and healthy controls. The area under the curve for miR-376a-3p was 0.651 revealing that the experimental results were reliable (**Figure 5C**). However, the role of miR-376a-3p during the progression of CAD remains unclear. Meanwhile, it has been shown that NRIP1 is also known as receptor-interacting protein 140 (RIP140), which plays an important role in regulating genes expression in heart [16]. Therefore, has-miR-376a-3p-NRIP1 pair was selected for further study.

Downregulation of miR-376a-3p inhibited proliferation of HUVECs

To investigate the role of miR-376a-3p in CAD, miR-376a-3p mimics or miR-376a-3p inhibitor was used. As shown in **Figure 6A**, the level of miR-376a-3p was markedly increased in HUVECs following transfection with miR-376a-3p mimics, and the level of miR-376a-3p was significantly decreased in cells following transfection with miR-376a-3p inhibitor (**Figure 6A**). In addition, CCK-8 and immunofluorescence assay results indicated that miR-376a-3p inhibitor obviously inhibited the proliferation of HUVECs (**Figure 6B-D**). Meanwhile, overexpression of miR-376a-3p significantly increased the proliferation of HUVECs (**Figure 6B**). These data indicated that downregulation of miR-376a-3p could inhibit the proliferation of HUVECs.

Downregulation of miR-376a-3p induced apoptosis of HUVECs

To further explore the function of miR-376a in CAD, flow cytometric assay was applied. As shown in **Figure 7A** and **7B**, miR-376a-3p inhibitor markedly induced the apoptosis of HUVECs, compared with the NC group. In addition, western blotting assay revealed that the expressions of Bax and cleaved caspase 3 were significantly increased, while the level of p-p65 was notably decreased in HUVECs following transfection with miR-376a-3p inhibitor, compared with the NC group (**Figure 7C-F**). These

Table 2. Enrichment analysis table of canonical pathway

Categories	Diseases or Functions Annotation	*p*-Value	Predicted Activation State	Activation z-score
Cellular Development, Cellular Growth and Proliferation	Development of tumor cell lines	1.26E-08		0.44
Organismal Injury and Abnormalities, Reproductive System Disease	Benign pelvic disease	5.74E-07		
Cellular Development, Cellular Growth and Proliferation	Cell proliferation of tumor cell lines	6.02E-07		0.184
Cancer, Gastrointestinal Disease, Hepatic System Disease, Organismal Injury and Abnormalities	Liver cancer	8.75E-07		
Cancer, Gastrointestinal Disease, Organismal Injury and Abnormalities	Upper gastrointestinal tract cancer	0.000001		
Cell Cycle	Interaction of DNA	1.3E-06		1.11
Cancer, Organismal Injury and Abnormalities	Pelvic tumor	1.44E-06		
Cancer, Organismal Injury and Abnormalities	Cancer of secretory structure	1.66E-06		
Cancer, Gastrointestinal Disease, Hepatic System Disease, Organismal Injury and Abnormalities	Liver carcinoma	1.81E-06		
Cancer, Gastrointestinal Disease, Hepatic System Disease, Organismal Injury and Abnormalities	Hepatobiliary system cancer	3.08E-06		
Cell Cycle, Gene Expression	Binding of DNA	4.01E-06		1.054
Cell Death and Survival, Cellular Function and Maintenance	Self-renewal of cells	4.3E-06		
Cancer, Organismal Injury and Abnormalities, Reproductive System Disease	Genital tumor	5.47E-06		
Immunological Disease	Systemic autoimmune syndrome	5.51E-06		
Cancer, Organismal Injury and Abnormalities	Pelvic cancer	6.37E-06		
Cancer, Gastrointestinal Disease, Organismal Injury and Abnormalities	Upper gastrointestinal carcinoma	7.42E-06		
Cell Death and Survival	Cell viability of tumor cell lines	7.7E-06		-0.482
Cancer, Organismal Injury and Abnormalities	Genitourinary tumor	8.57E-06		
Gastrointestinal Disease, Hepatic System Disease, Organismal Injury and Abnormalities	Liver lesion	1.31E-05		
Cell Death and Survival	Necrosis	1.32E-05		-0.769

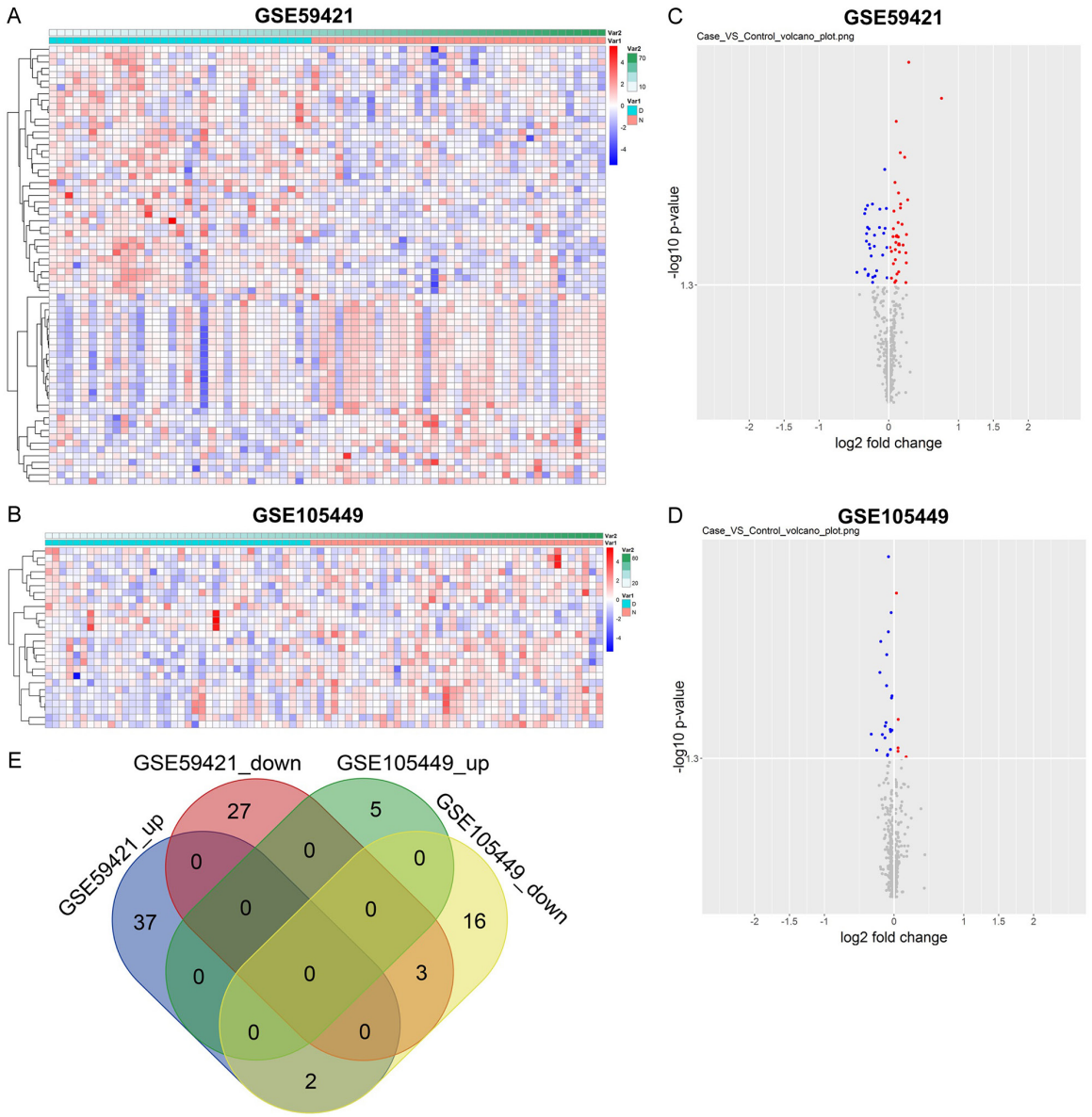

Figure 4. Identification of DEMs in GEO. Heat map showing the miRNA expression profiles of CAD samples and healthy controls according to *P* value, which downloaded from (A) GSE59421 dataset and (B) GSE105449 dataset. Red represented up-regulation, and blue indicated down-regulation. (C) Volcano plot of DEGs in GSE59421. (D) Volcano plot of DEGs in GSE105449. Gray, red and blue color represented relatively equal, high and low expression of genes respectively based on the cut-off values of |log2 fold change| >0 and -log10 (*p*-value) >1.3. (E) Venn diagram of overlapping DEGs from intersection of two independent datasets GSE59421 and GSE105449. A total of 0 upregulated and 3 downregulated overlapping DEMs was identified. Different colored regions represent different datasets.

results suggested that downregulation of miR-376a-3p could induce the apoptosis of HUVECs.

Overexpression of miR-376a-3p increased growth of HUVECs via downregulating NRIP1

Online bioinformatics tools miRWalk, RNA22 and TargetScan indicated that NRIP1 might be a potential target of miR-376a-3p (**Figure 8A**). In addition, dual luciferase reporter assay was applied to confirm whether NRIP1 was a binding target for miR-376a-3p. The results illustrated that miR-376a-3p mimics inhibited the luciferase activity of psiCHECK-2-NRIP1-WT, but it did not affect the luciferase activity of psiCHECK-2-NRIP1-MT (**Figure 8B**). These data

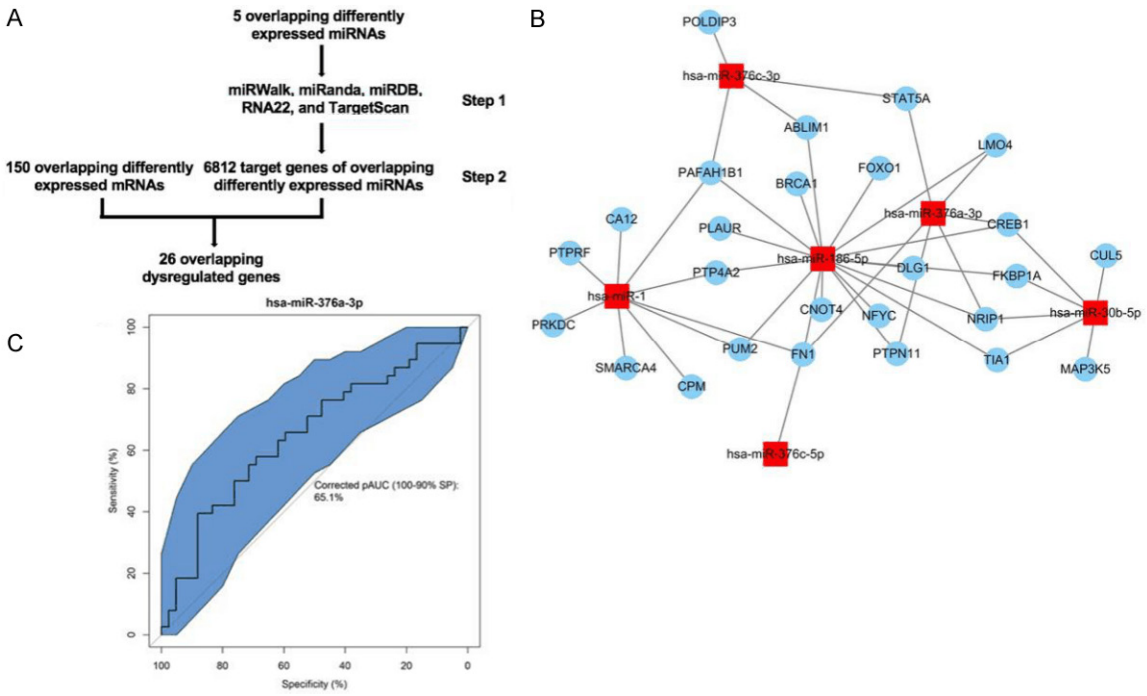

Figure 5. MiRNA-gene-network and module selection. A. Step 1, miRWalk, miRanda, miRDB, RNA22, and TargetScan predicting the potential target genes of differentially expressed miRNAs. Step 2, identifying the overlapping dysregulated genes from overlapping DEGs and miRNA target genes. B. miRNA-gene regulatory network of 43 miRNA-gene pairs. Blue circles denoted genes and red circles represented miRNA. Cytoscape version 3.3.0 software was used to plot the figure. C. Receiver operating characteristic analysis indicating the capacity of the miR-376a-3p to discriminate between patients with CAD and healthy controls.

Table 3. Function table of differential microRNA and differential RNA

microRNA	Degree	target gene	Degree
hsa-miR-186-5p	17	FN1	4
hsa-miR-1	9	CREB1	3
hsa-miR-376a-3p	6	NRIP1	3
hsa-miR-30b-5p	6	PAFAH1B1	3
hsa-miR-376c-3p	4	STAT5A	2
hsa-miR-376c-5p	1	FKBP1A	2

indicated that NRIP1 was a binding target of miR-376a-3p. Consistently, qRT-PCR assay indicated the level of NRIP1 was markedly downregulated in HUVECs following transfection with miR-376a-3p mimics (**Figure 8C**). Meanwhile, western blot assay illustrated that overexpression of miR-376a-3p significantly decreased the level of NRIP1, and increased the levels of p-p65, p-IκB in HUVECs (**Figure 8D-G**). These data illustrated that overexpression of miR-376a-3p increased growth of HUVECs via downregulating NRIP1.

Discussion

Evidence indicated that up- or downregulated miRNAs play a critical role in the progression of CAD [17]. However, the mechanism by which miRNAs regulate the levels of CAD-associated genes remains unclear. In this study, bioinformatics tools identified a total of 150 overlapping DEGs from datasets (GSE12288 and GSE20681), and 5 overlapping DEMs from datasets (GSE59421 and GSE105449) between patients with CAD and normal controls using R language. In addition, a multi-step method to identify the target genes of dysregulated miRNAs in CAD was performed (**Figure 5A**). First, miRNA and mRNA expression profiles were screened. After that, miRWalk, miRanda, miRDB, RNA22, and TargetScan were used to predict the target genes of DEMs. Thirdly, overlapping dysregulated genes from overlapping DEGs and miRNA target genes were identified. Finally, the present study further identified the interactions among miRNAs and overlapping dysregulated genes, 42 miRNA-gene pairs con-

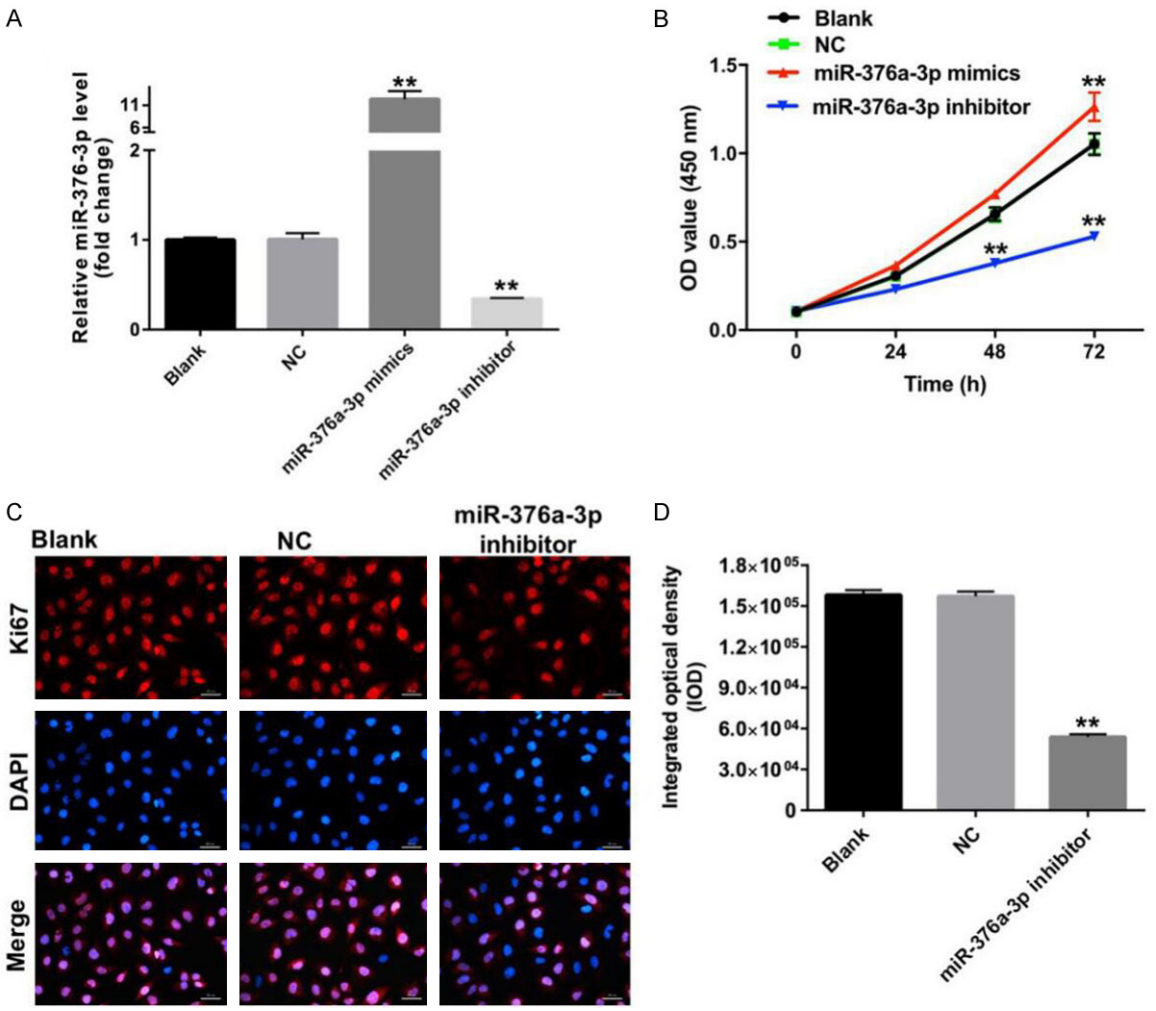

Figure 6. Downregulation of miR-376a-3p inhibited proliferation of HUVECs. A. HUVECs were transfected with 10 nM miR-376a-3p mimics or inhibitor for 72 h. RT-qPCR was used to detect the level of miR-376a-3p in HUVECs. **P<0.01 vs. NC group. B. HUVECs were transfected with 10 nM miR-376a-3p mimics or inhibitor for 24, 48 and 72 h. Cell viability was determined using CCK-8 assay. **P<0.01 vs. NC group. C. HUVECs were transfected with 10 nM miR-376a-3p inhibitor for 72 h. D. Relative fluorescence expressions were quantified by Ki67 and DAPI staining. The number of proliferating cells were counted. **P<0.01 vs. NC group.

taining 5 common DEMs and their target genes in CAD were identified (**Figure 5B**).

Previous study indicated that the expression of miR-376a-5p was markedly increased in the myocardial tissue of the CME pigs [18]. However, the role of miR-376a-3p and its downstream target are still unclear in CAD. For the first time, we found that miR-376a-3p was downregulated in CAD samples, compared with healthy controls. Bioinformatics analysis data indicated that NRIP1 was a potential target gene of miR-376a-3p. In addition, luciferase reporter assays validated that miR-376a-3p could directly target the 3'-UTR of NRIP1. These data illustrated that NRIP1 was a direct binding target of miR-376a-3p.

Nuclear receptor-interacting protein 1 (NRIP1) is also known as receptor-interacting protein 140 (RIP140), which is encoded by the NRIP1 gene [19]. It has been shown that RIP140 played an important role in regulating genes expression in heart [16]. Meanwhile, RIP140 was known as a deleterious mediator of energy metabolic homeostasis and cardiac mitochondrial function [20]. Chen et al. indicated that overexpression of RIP140 could activate apoptosis pathway in neonatal rat cardiomyocytes [21]. In this study, miR-376a-3p mimics signifi-

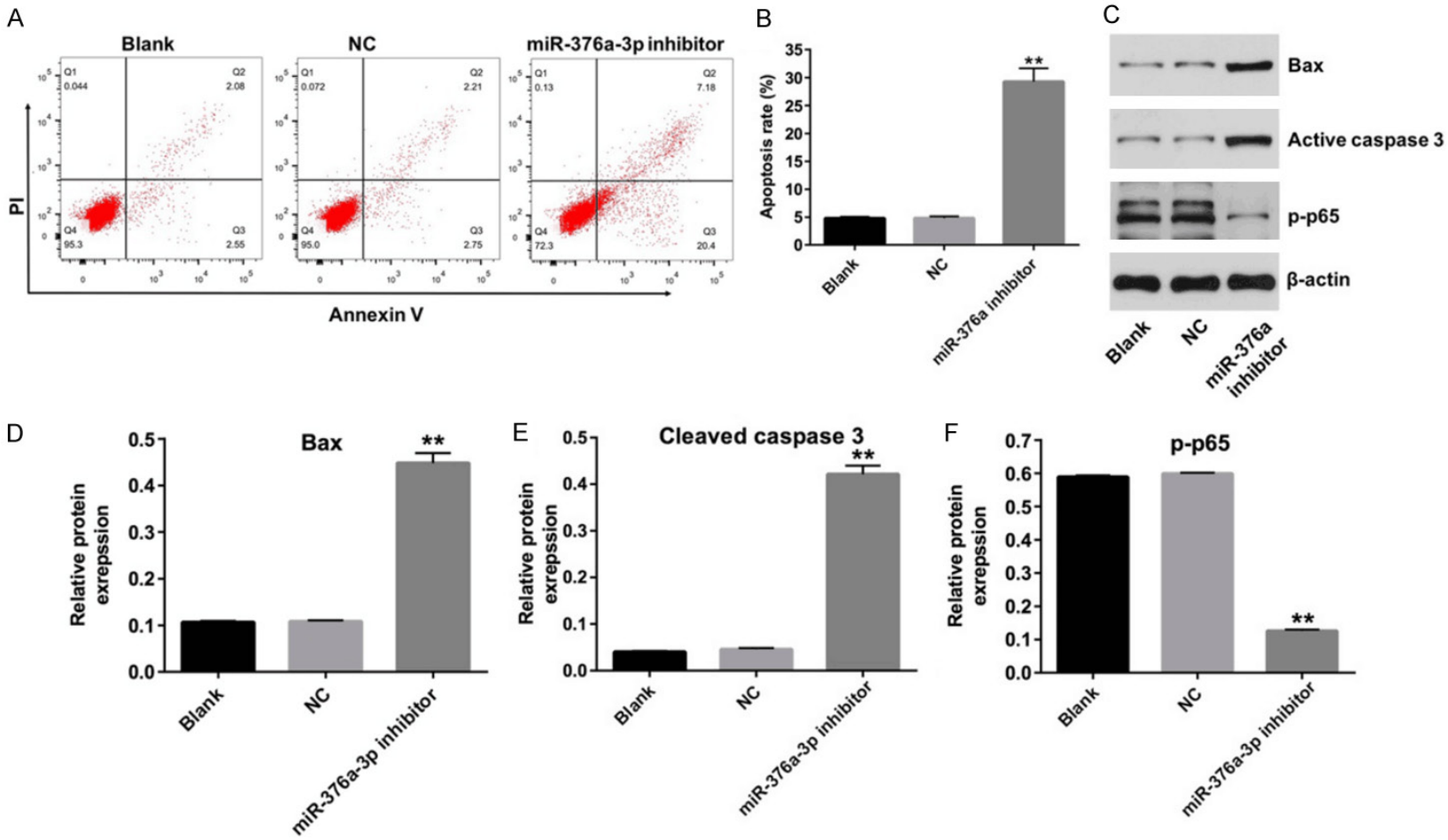

Figure 7. Downregulation of miR-376a-3p induced apoptosis of HUVECs. A, B. HUVECs were transfected with 10 nM miR-376a-3p inhibitor for 72 h. Apoptotic cells were detected with Annexin V and PI double staining. Apoptosis cell rates were calculated. **P<0.01 vs. NC group. C. Expression levels of Bax, cleaved caspase 3 and p-p65 in HUVECs were detected with western blotting. β-actin was used as an internal control. **P<0.01 vs. NC group. D-F. The relative expressions of Bax, cleaved caspase 3 and p-p65 were quantified via normalization to β-actin. **P<0.01 vs. NC group.

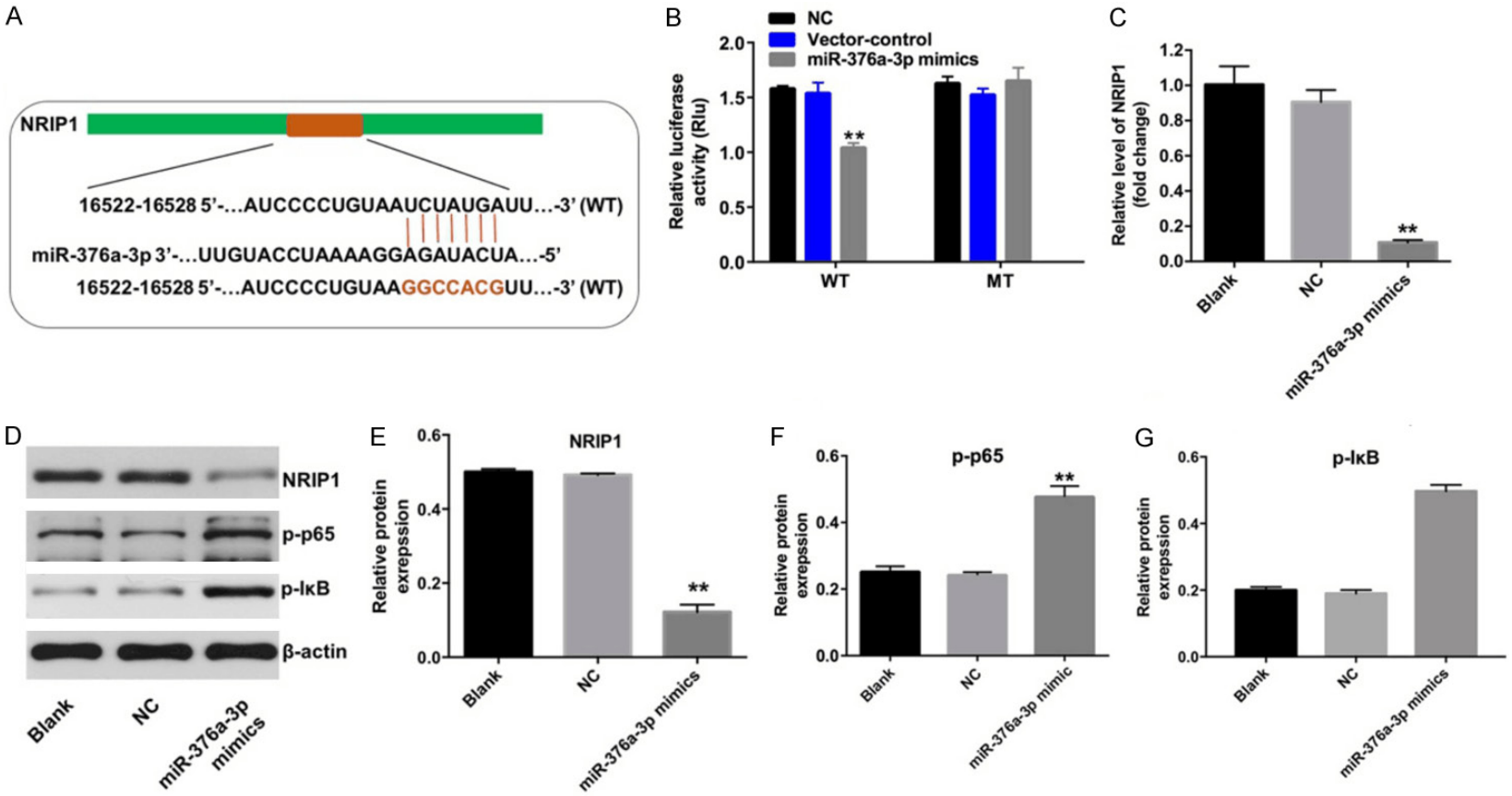

Figure 8. Overexpression of miR-376a-3p increased growth of HUVECs via downregulating NRIP1. A. Sequence alignment of miR-376a-3p with the putative binding sites within the WT regions of NRIP1. B. Dual luciferase reporter assay was used to detect the luciferase activity in HUVECs following co-transfecting with NRIP1-WT/MUT 3'-UTR plasmid and miR-376-3p mimics. **P<0.01 vs. vector-control group. C. HUVECs were transfected with 10 nM miR-376a-3p mimics for 72 h. RT-qPCR was used to detect the level of NRIP1 in HUVECs. D. Expression levels of NRIP1, p-p65 and p-IκB in HUVECs were detected with western blotting. β-actin was used as an internal control. E-G. The relative expressions of NRIP1, p-p65 and p-IκB in HUVECs were quantified via normalization to β-actin. **P<0.01 vs. NC group.

cantly decreased the level of NRIP1 in HUVECs. Meanwhile, downregulation of miR-376a-3p could induce the apoptosis in HUVECs. These data might suggest that downregulation of NRIP1 could inhibit apoptosis in HUVECs. In addition, we found that overexpression of miR-376a-3p markedly increased the levels of p-NF-κB (p65) and p-IκB in HUVECs. Liao et al. found that NF-κB-p65 could inhibit myocardin-induced cardiomyocyte hypertrophy [22]. Thus, it may be suggested that overexpression of miR-376a could attenuate progression of CAD via downregulating of NRIP1, and then activation of p65.

Conclusion

In this study, several DEGs and DEMs were identified by integrating GEO datasets. In addition, miR-376a-3p-NRIP1 pair might involve in the progression of CAD. Moreover, miR-376a-3p might be a therapeutic target for the treatment of CAD.

Disclosure of conflict of interest

None.

Address correspondence to: Xuhui Wang, Department of Neurosurgery, Xinhua Hospital Affiliated to Shanghai Jiao Tong University School of Medicine, No. 1665 Kongjiang Road, Yangpu District, Shanghai 200092, P. R. China. E-mail: wangxuhui@xinhuamed.com.cn; Fang Liu, Department of Gerontology, Xinhua Hospital Affiliated to Shanghai Jiao Tong University School of Medicine, No. 1665 Kongjiang Road, Yangpu District, Shanghai 200092, P. R. China. E-mail: liufang@xinhuamed.com.cn

References

[1] Mordi IR, Badar AA, Irving RJ, Weir-McCall JR, Houston JG and Lang CC. Efficacy of noninvasive cardiac imaging tests in diagnosis and management of stable coronary artery disease. Vasc Health Risk Manag 2017; 13: 427-437.

[2] Demir V, Yilmaz S, Ede H and Turan Y. Correlation of resting heart rate with the severity and complexity of coronary artery disease: a single-center retrospective study. Int J Prev Med 2019; 10: 104.

[3] Wong ND. Epidemiological studies of CHD and the evolution of preventive cardiology. Nat Rev Cardiol 2014; 11: 276-289.

[4] Ramadhani FB, Liu Y, Jing X, Qing Y, Rathnayake AK, Kara WSK and Wu W. Investigating the relevance of nursing caring interventions delivered to patients with coronary artery disease at a teaching hospital in china: a retrospective study. Cureus 2019; 11: e4672.

[5] Risavi BL and Staszko J. Prevalence of risk factors for coronary artery disease in pennsylvania (USA) firefighters. Prehosp Disaster Med 2016; 31: 102-107.

[6] Saleh-Ghadimi S, Kheirouri S, Golmohammadi A, Moludi J, Jafari-Vayghan H and Alizadeh M. Effect of flaxseed oil supplementation on anthropometric and metabolic indices in patients with coronary artery disease: a double-blinded randomized controlled trial. J Cardiovasc Thorac Res 2019; 11: 152-160.

[7] Hamrefors V. Common genetic risk factors for coronary artery disease: new opportunities for prevention? Clin Physiol Funct Imaging 2017; 37: 243-254.

[8] Deb S, Wijeysundera HC, Ko DT, Tsubota H, Hill S and Fremes SE. Coronary artery bypass graft surgery vs percutaneous interventions in coronary revascularization: a systematic review. JAMA 2013; 310: 2086-2095.

[9] Zhao X, Jia Y, Chen H, Yao H and Guo W. Plasma-derived exosomal miR-183 associates with protein kinase activity and may serve as a novel predictive biomarker of myocardial ischemic injury. Exp Ther Med 2019; 18: 179-187.

[10] Tan X, Zhang X, Pan L, Tian X and Dong P. Identification of key pathways and genes in advanced coronary atherosclerosis using bioinformatics analysis. Biomed Res Int 2017; 2017: 4323496.

[11] Zhu J, Wang Z and Chen F. Association of key genes and pathways with atopic dermatitis by bioinformatics analysis. Med Sci Monit 2019; 25: 4353-4361.

[12] Yu C, Chen F, Jiang J, Zhang H and Zhou M. Screening key genes and signaling pathways in colorectal cancer by integrated bioinformatics analysis. Mol Med Rep 2019; 20: 1259-1269.

[13] Jin Y and Yang Y. Identification and analysis of genes associated with head and neck squamous cell carcinoma by integrated bioinformatics methods. Mol Genet Genomic Med 2019; e857.

[14] Wang W, Xu Z, Zhu X and Chang X. Mining the potential therapeutic targets for coronary artery disease by bioinformatics analysis. Mol Med Rep 2018; 18: 5069-5075.

[15] White TE and Ford BD. Frontiers in neuroengineering gene interaction hierarchy analysis can be an effective tool for managing big data related to unilateral traumatic brain injury. In: Kobeissy FH, editors. Brain neurotrauma: molecular, neuropsychological, and rehabilitation aspects. Boca Raton (FL): CRC Press/Taylor & Francis (c) 2015 by Taylor & Francis Group, LLC.; 2015.

[16] Fritah A, Steel JH, Nichol D, Parker N, Williams S, Price A, Strauss L, Ryder TA, Mobberley MA, Poutanen M, Parker M and White R. Elevated expression of the metabolic regulator receptor-interacting protein 140 results in cardiac hypertrophy and impaired cardiac function. Cardiovasc Res 2010; 86: 443-451.
[17] Rizzacasa B, Morini E, Mango R, Vancheri C, Budassi S, Massaro G, Maletta S, Macrini M, D'Annibale S, Romeo F, Novelli G and Amati F. MiR-423 is differentially expressed in patients with stable and unstable coronary artery disease: a pilot study. PLoS One 2019; 14: e0216363.
[18] Su Q, Li L, Zhao J, Sun Y and Yang H. MiRNA expression profile of the myocardial tissue of pigs with coronary microembolization. Cell Physiol Biochem 2017; 43: 1012-1024.
[19] Cavailles V, Dauvois S, L'Horset F, Lopez G, Hoare S, Kushner PJ and Parker MG. Nuclear factor RIP140 modulates transcriptional activation by the estrogen receptor. EMBO J 1995; 14: 3741-3751.
[20] You J, Yue Z, Chen S, Chen Y, Lu X, Zhang X, Shen P, Li J, Han Q, Li Z and Liu P. Receptor-interacting protein 140 represses Sirtuin 3 to facilitate hypertrophy, mitochondrial dysfunction and energy metabolic dysfunction in cardiomyocytes. Acta Physiol (Oxf) 2017; 220: 58-71.
[21] Chen Y, Wang Y, Chen J, Chen X, Cao W, Chen S, Xu S, Huang H and Liu P. Roles of transcriptional corepressor RIP140 and coactivator PGC-1alpha in energy state of chronically infarcted rat hearts and mitochondrial function of cardiomyocytes. Mol Cell Endocrinol 2012; 362: 11-18.
[22] Liao XH, Wang N, Zhao DW, Zheng DL, Zheng L, Xing WJ, Zhou H, Cao DS and Zhang TC. NF-kappaB (p65) negatively regulates myocardin-induced cardiomyocyte hypertrophy through multiple mechanisms. Cell Signal 2014; 26: 2738-2748.